RSC Advances

ROYAL SOCIETY OF CHEMISTRY

www.rsc.org/advances

Journal Name

ARTICLE

Electrospun porous $CuCo_2O_4$ nanowire networks electrode for asymmetric supercapacitor

Received 00th January 20xx,
Accepted 00th January 20xx

DOI: 10.1039/x0xx00000x

www.rsc.org/

Qiufan Wang,[a*] Di Chen[b], and Daohong Zhang[a*]

Porous network nanostructures have been demonstrated as one of the most ideal electrode materials in energy storage systems due to their advantages of both microstructures and their high surface area. In this study, a facile electrospinning method with subsequent heat treatments is employed to firstly prepare $CuCo_2O_4$ network structure. The $CuCo_2O_4$ network electrode delivers a remarkable areal capacitance of 443.9 mF/cm^2 at a current density of 1 mA/cm^2. The electrode also presents excellent cyclic stability of 90% capacity retention after 1500 cycles at 1 mA/cm^2. We have successfully fabricated high-performance asymmetric supercapacitor based on $CuCo_2O_4$ network nanostructure and active carbon as positive and negative materials, respectively. The assembled novel asymmetric supercapacitor device with an extended operating voltage window of 1.5 V exhibits excellent performance such as a high energy density of 0.806 mWh/cm^3 and good rate capability. The high-performance nanostructured $CuCo_2O_4$ has significant potential applications in electrical vehicles.

Introduction

Due to the rapidly growing global energy consumption and worsened environmental pollution, the development of green power sources has become an urgent and increasing demand in various fields such as electric vehicles, hybrid electric vehicles, and other power-supply devices.[1,2] Among various energy storage devices, supercapacitor, with high power density, fast charge/discharge rate, and long lifespan, is typically considered as one of the most appropriate choice for energy storage devices.[3-5] In order to meet the increasing energy density demands for next generation electronic devices, the energy density of supercapacitor needs to be further improved. According to the equation of energy density ($E=0.5CV^2$), the specific energy density can be improved by increasing the output voltage and/or the specific capacitance.[6-7] Asymmetric supercapacitor can combine a battery-tape Faradaic electrode and a capacitor-type electrode to increase the output voltage. Thus, developing appropriate electrode materials has become the essential part of the current endeavor to boost the energy densities of asymmetric supercapacitors.[8-11]

Among the multitudinous available pseudocapacitive materials, transition metal oxides are considered especially promising as electrode materials, due to their multiple oxidation state, excellent intrinsic properties and good electrochemical performance.[12-13] Building the porous 3D nanostructure is a promising solution to achieve high capacitance. From a wide range of pseudocapacitive materials, spinel oxides have a high electronic/ionic conductivity and catalytic activity, that are of great interest for energy storage applications.[14-17] We have got some important achievements in this area,[13a,17] a core/shell $CuCo_2O_4$@MnO_2 heterostructured nanowire array on carbon fabrics have been firstly fabricated as electrode for symmetric supercapacitor, and a maximum specific capacitance of 327 F/g was achieved.[18]

$CuCo_2O_4$ (CCO) is a binary spinel metal oxide with great electronic conductivity and electrochemical activity than single-component copper or cobalt oxide. Recently research on nanosructured materials has demonstrated enhanced capacitive performance, because of their high surface area, short ion-diffusion path, and fast kinetics. Therefore, rationally designed the morphology and/or structure provides one of the most feasible ways to create high performance supercapacitors. Wang et al. synthesized grass-like $CuCo_2O_4$ nanowire arrays on Ni foam to achieve a high area capacitance of 611 F/g at current density of 1.7 A/g.[19] Luo et al. recently reported mesoporous $CuCo_2O_4$ nanograsses on copper foam with an excellent specific capacitance of 796 F/g at a current density of 2 A/g.[20] Compared with the above processes, electrospinning is a cost-effective, versatile, and simple way to fabricate well-defined 3D nanostructures.

Herein, we firstly propose and realize a facile, effective, and scalable strategy for preparing spinel-based porous $CuCo_2O_4$ network by combing the electrospinning technique with a heating method. The new network $CuCo_2O_4$ structure is firstly investigated as the supercapacitor electrode materials. Electrochemical measurements show that this network electrode can exhibit excellent specific capacitance as high as 443.9 mF/cm^2. Then, we fabricate asymmetric supercapacitors with $CuCo_2O_4$ and active

[a] Key Laboratory of Catalysis and Materials Science of the State Ethnic Affairs Commission & Ministry of Education, South-Central University for Nationalities, Wuhan, Hubei Province, 430074, China.
[b] School of Mathematics and Physics, University of Science and Technology Beijing, Beijing 100083, China. E-mail:chendi@ustb.edu.cn
* Dr Q. F. Wang, YGDF@mail.scuec.edu.cn
*Dr. D.H. Zhang, Zhangdh27@163.com.
Electronic Supplementary Information (ESI) available. See DOI: 10.1039/x0xx00000x

carbon as two electrodes for practical applications. It is found that this asymmetric supercapacitor could deliver a high energy density of 0.806 mWh/cm^3 at power density of 7.8 mW/cm^3, and good rate capability. The high-performance $CuCo_2O_4$ nanostructures may have significant potential applications in electrical vehicles.

Experimental

Synthesis of $CuCo_2O_4$ nanowire networks.

All chemical reagents were used of analytical grade and were used directly without any purification. In a typical procedure, poly(vinylpyrolidone) (PVP, M_W=130000 g/mol) was dissolved in a mixture of ethanol (5mL) and *N*, *N*-dimethylformamide (DMF, 5mL) with vigorous stirring to form a 10 wt% solution. Then, 0.4748 g $Co(NO_3)_2 \cdot 6H_2O$ and 0.1128 g $Cu(NO_3)_2 \cdot 6H_2O$ were added in the above solution. After stirring at room temperature for 12 h, the precursor solution was obtained. Subsequently, the above precursor solution was drawn into a hypodermic syringe. The positive terminal of a variable high-voltage power supply was connected to the needle tip of the syringe, while the other terminal was connected to the collector plate. With a flow rate of 1 mL h^{-1} and an applied voltage of 18 kV between the needle tip and aluminum collector with a distance of 15 cm, the as-prepared solution was electrospun into nanowires. Afterward, the above spun nanowires were sintered at 500 ^{o}C for 3 h at a rate of 2 ^{o}C/min in air.

Fabrication of working electrode.

The working electrode was prepared by mixing the as-prepared $CuCo_2O_4$ nanowire network (or active carbon), acetylene black, and polyvinylidene fluoride (PVDF) binder with a weight ratio of 70:20:10, which were pasted onto a treated nickel foam and dried under a vacuum at 100 ^{o}C for 5 h to remove NMP.

Fabrication of $CuCo_2O_4$//active carbon asymmetric supercapacitors.

The fabrication of the $CuCo_2O_4$//active carbon (AC) asymmetric supercapacitors was conducted by taking the $CuCo_2O_4$ network and AC as positive and negative electrodes, respectively. A 3 M KOH solution was used as the electrolyte, and a glass membrane as the separator in two-electrode simulation cells. The thickness of the device was measured to be 1 mm, including the electrodes and the separator.

Electrochemical measurements.

The electrochemical tests were carried out at room temperature in both three-electrode and two-electrode configurations. In the three-electrode system, the as-prepared $CuCo_2O_4$ positive electrode (or active carbon negative electrode), a platinum electrode, and a saturated calomel electrode (SCE) were used as the working electrode, counter electrode, and reference electrode, respectively. A 3 M KOH solution was used as electrolyte for all electrochemical measurements. The electrochemical performances were measured with an electrochemical workstation (CHI760D). The electrochemical properties and capacitive behavior of the electrochemical properties and capacitive behavior of the supercapacitor electrodes were evaluated by cyclic voltammetry (CV) and galvanostatic charge-discharge (CD). EIS measurements were carried out in the frequency range from 0.01 Hz to 100 KHz.

The calculation of energy and power density is based on the total weight of the two electrodes in the full-cell devices according to the following equations.

Calculations.

The energy density (Wh/cm^3) and power density (W/cm^3) derived from galvanostatic charge/discharge curves are estimated by following equations:

$$E=C\times\Delta V^2/(2\Delta V\times 3600) \quad (1)$$

$$P=E\times 3600/\Delta t \quad (2)$$

Where ΔV is the potential drop during discharge.

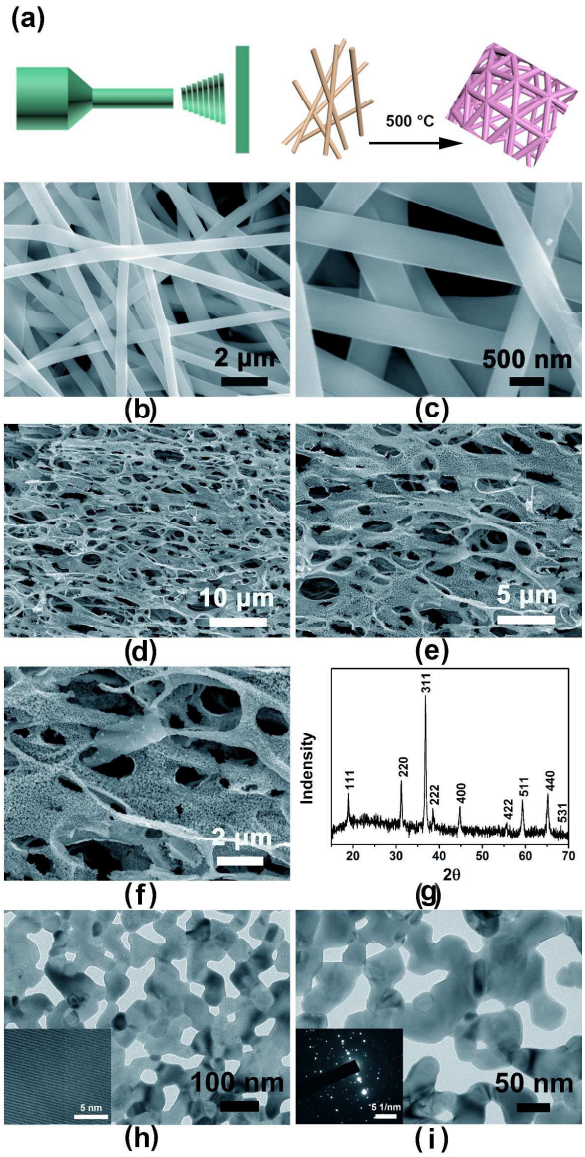

Figure 1. (a) Schematic illustration of the growth mechanism of $CuCo_2O_4$ network nanostructures. (b, c) SEM images of the $CuCo_2O_4$ nanowire precursor. (d-f) SEM images of the $CuCo_2O_4$ nanowires network after calcination. (g) XRD pattern of $CuCo_2O_4$ nanowire network. (h, i) TEM images of the $CuCo_2O_4$ nanowires, the insets are high-resolution TEM and SAED images, respectively.

Materials characterizations.

The synthesized products were characterized with an X-ray diffractometer (XRD; X'Pert PRO, PANalytical B.V., the Netherlands) with radiation from a Cu target (Kα, λ= 0.15406 nm). The morphologies of the samples were characterized using electron microscopy (FESEM; JEOL JSM-6700F, 5 kV) and transmission electron microscopy (HRTEM; JEOL JEM-2010 HT) coupled with an energy-dispersive X-ray spectrometer (EDX).

Results and discussion

Figure 1a schematically illustrates the facile synthetic process of $CuCo_2O_4$ network nanostructures. The morphology and detailed structural information are determined by scanning electron microscopy (SEM) and transmission electron microscopy (TEM). Figure 1b, c show the as-spun nanofibers before the calcination. It could be observed that these nanowires have a smooth and uniform surface. Their lengths could reach dozens of micrometers, and the diameter ranged from 450 to 500 nm. After calcination in air for 3 h, the $CuCo_2O_4$ webs maintain the interconnected porous network microstructure as shown in Figure 1d-f. Figure 1h, i show the TEM images of the network structure, which reveal clearly that the network is composed by a large amount of connect nanocrystallites with sizes of 30-50 nm. A lot of uniform separated nanopores exist among these nanoparticles and are absolutely penetrated. In order to obtain the microstructure of $CuCo_2O_4$ nanowire network, the high-resolution transmission electron microscopy (HRTEM) observations were carried out, and the corresponding results are shown in the inset of Figure 1g. The diffraction ring pattern of the selected-area electron diffraction (SAED) indicates the polycrystalline assembling nature of the network (inset of Figure 1h). X-ray photoelectron spectroscopy (XPS) survey spectrums of the Cu, Co and O element show in Figure 2. The XPS Cu 2p and Co 2p spectra indicate that copper exist in the Cu^{2+} state and cobalt has a spinel structure.[21]

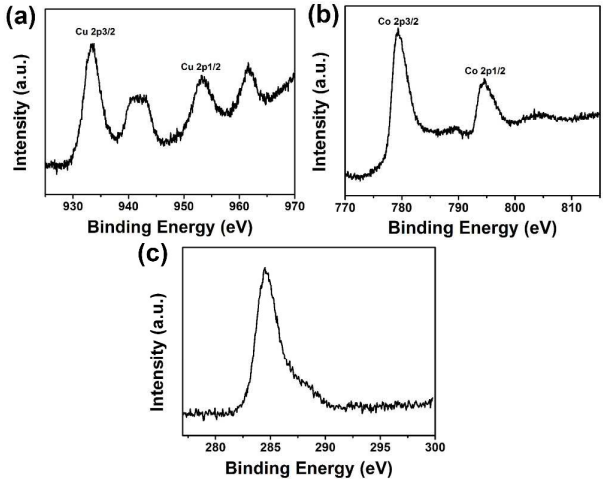

Figure 2. (a) XPS Cu 2p, (b) XPS Co 2p, and (c) XPS C1s.

The electrochemical properties of $CuCo_2O_4$ nanowire network electrode material for SC were performed with three-electrode test system (Figure 3a). Figure 3b shows representative CV curves of $CuCo_2O_4$ network structure in a aqueous electrolyte of 3 M KOH from 0 to 0.42 V (*vs*. SCE). A pair of strong redox peaks were visible in each voltammogram indicating that the capacitance characteristics are mainly governed by Faradaic redox reactions. At a low scan rate of 5 mV/s, the anodic peak at 0.276 V is due to the oxidation process, and the cathodic peak at about 0.158 V is related to its reverse process. A possible mechanism is that by initiating the scan from cathodic potentials, CoOOH[22a] and CuOH may form at the outer surface of the $CuCo_2O_4$ electrode, according to the following equation[22c]:

$$CuCo_2O_4+H_2O+e^- \leftrightarrow 2CoOOH+Cu(OH)^- \quad (3)$$

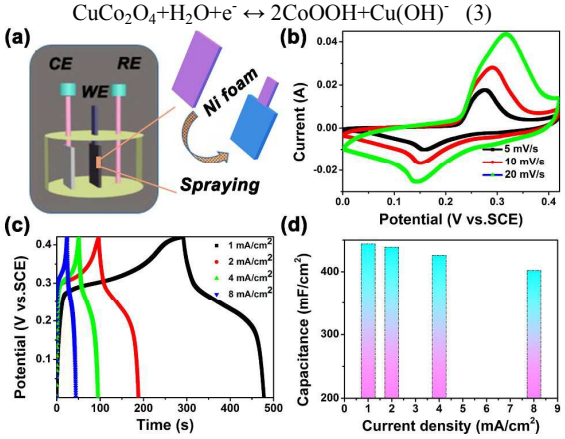

Figure 3. (a) The diagram of the three-electrode test system. (b) CV curves for $CuCo_2O_4$ network at different scan rates. (c) Galvanostatic charge/discharge curves for $CuCo_2O_4$ network at different current densities. (d) Areal capacitance of $CuCo_2O_4$ networks versus discharge current.

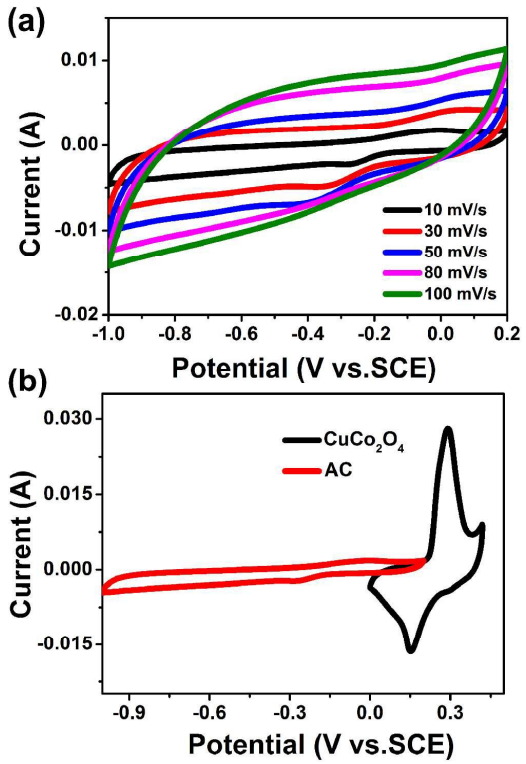

Figure 4. (a) Active carbon electrode at different scan rates, (b) comparative CV curves of $CuCo_2O_4$ and active carbon electrodes obtained in a three-electrode system in 3 M KOH aqueous solution at a scan rate of 10 mV/s.

Journal Name

ARTICLE

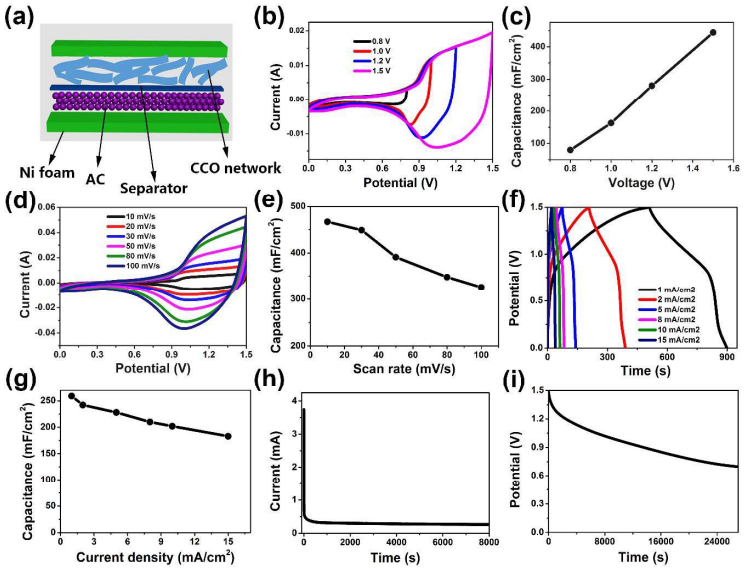

Figure 5. (a) Schematic presentation of asymmetric supercapacitor. (b) CV curves tested over different voltages from 0.8 to 1.5 V. (c) Specific capacitance variation with voltage. (d) CV curves of an optimized asymmetric supercapacitor at scan rates ranging from 10 to 100 mV/s. (e) Specific capacitance variation with scan rate. (f) Galvanostatic charge/discharge curves obtained over different current densities. (g) Specific capacitance variation with current density. (h) Leakage current curve. (i) Self-discharge curve of the device after charging at 1.5 V.

Then, by sweeping the potential toward positive values, redox reactions occur as follows:

$$CoOOH+OH^- \leftrightarrow CoO_2+H_2O+e^- \quad (4)$$

$$CuOH+OH^- \leftrightarrow Cu(OH)_2+e^- \quad (5)$$

The peak current increases linearly with the scan rate, suggesting that the rates of electronic and ionic transport should be rapid enough in the applied scan rates. Figure 3c shows the galvanostatic charge/discharge curves at different current densities ranging from 1 to 8 mA/cm^2.

The specific capacitance C (mF cm^{-2}), one of the most important parameters for characterizing the electrochemical performance of capacitors, can be calculated from the discharge curve according to $C= I\Delta t/(S\Delta V)$ (mF/cm^2). Where I is the discharge current, Δt is the discharge time, S is the area of the active material and ΔV is the potential window during discharge curve.

The areal capacitance versus discharge current density is plotted in Figure 3d. The specific capacitances of the $CuCo_2O_4$ network are calculated to be 443.9, 439, 426 and 402 mF/cm^2, at current densities of 1, 2, 4 and 8 mA/cm^2. With increasing current density, the specific capacitance decreases gradually, we can obtain the specific capacitance of 402 mF/cm^2 for the $CuCo_2O_4$ network at high current density of 8 mA/cm^2, representing only 9.5% decrease compared with the specific capacitance of 443.9 mF/cm^2 at a current density of 1 mA/cm^2, which is comparable with the previous report,[22b] and lower than the binder-free $NiMoO_4$ nanoplate arrays-based asymmetric supercapacitor,[22d] and $CoMoO_4$ nanosheet.[22e] This result indicates the excellent capacitive behavior and high-rate capability of the $CuCo_2O_4$ network nanostructure.

The superior electrochemical performance of $CuCo_2O_4$ electrode can be attributed to the network structure providing large accessible surface area, fast ion and electron transfer, and good structural stability. Significantly, the excellent capacitive behaviors demonstrate that the as-prepared network $CuCo_2O_4$ will be a promising candidate as a positive electrode for asymmetric supercapacitors.

To identify the potential window of asymmetric supercapacitor and balance the charges between positive and negative electrodes, we also investigate the electrochemical performance of active carbon electrode in a three-electrode system. The active carbon electrode shows a potential window of -1 V to 0.2 V, Figure 4a demonstrates the CV curves of AC electrode at different scan rates. Figure 4b shows the comparison of CV curves for two electrodes at a scan rate of 10 mV/s. To achieve the optimized performance of the asymmetric device, the optimal mass ratio of positive and negative electrode is fixed to around 0.65:1, which is based on the charge balance between the two electrodes.

To further evaluate the $CuCo_2O_4$ network electrode for practical application, a simple asymmetric supercapacitor device is manufactured by using the $CuCo_2O_4$ and active carbon electrodes. Figure 5a displays the schematic illustration for the device. Figure

5b demonstrates the CV curves collected at 30 mV/s in different voltage windows for the $CuCo_2O_4$//AC ASC. The calculated values of specific capacitance are displayed in Figure 5c as a function of operating voltage window. A series of CV measurements at different scan rates from 10 to 100 mV/s is displayed in Figure 5d. The current increases with the scan rate increasing, but the shape is well retained, indicating its ideal capacitive nature. The gradual fall of specific capacitance with increasing scan rate is clearly apparent form Figure 5e, which is the consequence of diffusion limits in charge transport at higher scan rates. The specific capacitance increases from 326 mF/cm^2 to 467 mF/cm^2 with the scan rate from 100 to 10 mV/s.

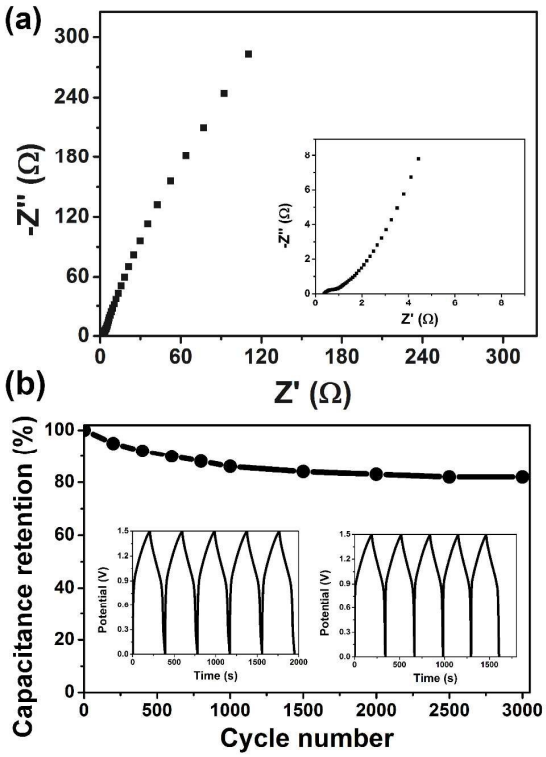

Figure 6. (a) Nyquist plots for asymmetric device. (b) Cycling performance of the asymmetric device. The inset were the charge/discharge curves for the first and last five cycles.

Figure 5f demonstrate the galvanostatic charge/discharge measurements, which are carried out at different current densities in the potential window of 0-1.5 V. The specific capacitances are calculated at different current densities and plotted in Figure 5g. The device shows an excellent rate capability and the areal capacitance can still be maintained at 183 mF/cm^2 even when the current density increased 15 times from 1 to 15 mA/cm^2, which is higher than the reported value of NiO//rGO-based ASC.[27] Meanwhile, our fabricated asymmetric supercapacitor reveals a low leakage current of 0.26 mA (Figure 5h), and an open circuit voltage of 0.7 V can be maintained for 7.44 h after charged at 1.5 V (Figure 5i).

The Nyquist plot in Figure 6a represents excellent electrical conductivity of the device with a very small cell resistance shown at a high frequency range. The disappearance of the semicircle in the Nyquist plot in a high frequency range exhibited very small charge/discharge resistance of the device, which is probably ascribed to the integrated 3D electrodes that minimize the contact impedance between electrodes and electrolyte.

The long-term cycling performance is one of the most critical factors to determine the energy storage performance for supercapacitor operations. The cycling test of our asymmetric devices is evaluated in the 1.5 V voltage window at a current density of 2 mA cm^{-2} for 3000 cycle (Figure 6b), it shows about 82% capacitance retention, which is significantly better than those reported in previous work (typical 70-85% retention over 3000 cycle).[23-26] The capacity decay after long-term cycling for our asymmetric device may due to the mechanical failure of the $CuCo_2O_4$ electrode, resulting in the delamination of the active materials from the Ni foam substrate.

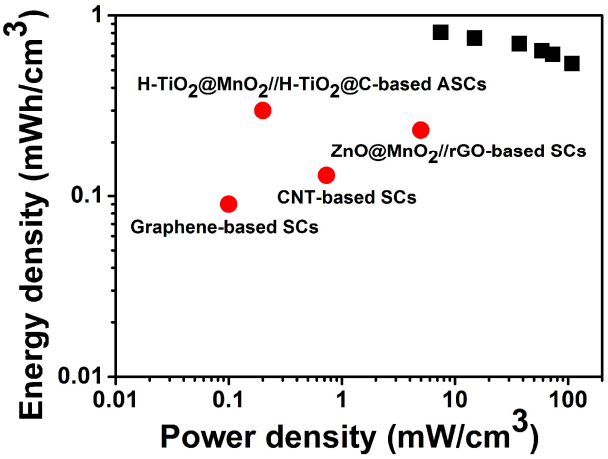

Figure 7. Ragone plots of the asymmetric supercapacitor based on the full cell. The values reported for other supercapacitors are added for comparison.

The energy and power densities are two key parameters in characterizing the performances of supercapacitors. Figure 7 shows the Ragone plot of our asymmetric supercapacitors . The maximum energy density of the prepared ASC is 0.81 mWh/cm^3 at a power density of 7.48 mW/cm^3. These values are superior to the previously reported supercapacitor systems, including ZnO@MnO_2//rGO-based SCs (0.234 mWh/cm^3, 5 mW/cm^3),[28] H-TiO_2@MnO_2//H-TiO_2@C-based ASCs (0.3 mWh/cm^3 at 0.2 W/cm^3),[29] and CNT-based supercapacitors with 0.13 mWh/cm^3 at 0.73 W/cm^3,[30] also are about 9-fold higher than graphene-based SCs (0.09 mWh/cm^3 at 0.1 W/cm^3)[31] The excellent performance can attribute to the large surface area that leads to sufficient ion transfer on electrode/electrolyte interface, also the nanopores on the surface can supply facile transport channel for OH^- ions. On the other hand, the interconnected webs provide a continuous pathway for electron transport. The high energy and power densities of our asymmetric supercapacitors are of great promise of practical energy storage applications.

Conclusions

In summary, a facile electrospinning method is used to fabricate the $CuCo_2O_4$ network structure. The $CuCo_2O_4$ network on the Ni foam substrate serve as an excellent three-dimensional supercapacitor electrode, showing a specific capacitance and

excellent rate capability and conductivity. Furthermore, the asymmetric supercapacitor fabricated by the optimized $CuCo_2O_4$ network as positive electrode and active carbon as negative electrode demonstrates outstanding electrochemical performance. Our asymmetric supercapacitor shows high energy and power density, as well as robust long-term cycling stability. The performance we achieved suggests that the ternary $CuCo_2O_4$ prepared by electrospinning process have great potential in various energy storage technologies.

Acknowledgements

We gratefully acknowledge the financial support of Hubei Province Natural Science Fund for Distinguished Young Scientists (2014CFA037)..

Notes and references

‡ Footnotes relating to the main text should appear here. These might include comments relevant to but not central to the matter under discussion, limited experimental and spectral data, and crystallographic data.

1 J. R. Miller and P. Simon, Science, 2008, 321, 651.
2 K. S. Kang, Y. S. Meng, J. Breger, C. P. Grey and G. Ceder, Science, 2006, 311, 977.
3 (a) H. Zhao, C. Wang, R. Vellacheri, M. Zhou, Y. Xu, Q. Fu, M. Wu, F. Grote and Y. Lei , Adv. Mater. 2014, 26, 7654, (b) D. Zhang, M. Miao, H. Niu and Z. Wei, ACS Nano, 2014, 8, 4571-4579.
4 (a) J. Zhao, H. Lai, Z. Lyu, Y. Jiang, K. Xie, X. Wang, Q. Wu, L. Yang, Z. Jin, Y. Ma, J. Liu and Z. Hu, Adv. Mater., 2015, 27, 3541, (b) C. Z. Yuan, L. Yang, L. R. Hou, L. F. Shen, X. G. Zhang and X. W. Lou, Energy Environ. Sci., 2012, 5, 7883-7887.
5 E. Lim, H. Kim, C. Jo, J. Chun, K. Ku, S. Kim, H. I. Lee, I.-S. Nam, S. Yoon, K. Kang and J. Lee, ACS Nano, 2014, 8, 8968.
6 P. C. Chen, G. Z. Shen, Y. Shi, H. Chen and C. W. Zhou, ACS Nano, 2010, 4, 4403-4411.
7 J. Xu, Q. F. Wang, X. W. Wang, Q. Y. Xiang, B. Liang, D. Chen and G, Z. Shen, ACS Nano, 2013, 7, 5453-5462.
8 N. S. Choi, Z. H. Chen, S. A. Freunberger, X. L. Ji, Y. K. Sun, K. Amine, G. Yushin, L. F. Nazar, J. Cho and P. G. Bruce, Angew. Chem. Int. Edit., 2012, 51, 9994.
9 J. B. Goodenough and K. S. Park, J. Am. Chem. Soc., 2013, 135, 1167.
10 L. W. Ji, Z. Lin, M. Alcoutlabi and X. W. Zhang, Energy Environ. Sci., 2011, 4, 2682.
11 L.Yu, L. Zhang, H. B. Wu, G. Q. Zhang and X. W. Lou, Energy Environ. Sci., 2013, 6, 2664-2671.
12 V. Augustyn, P. Simon and B. Dunn, Energy Environ. Sci., 2014, 7, 1597.
13 Q. F. Wang, X. F. Wang, B. Liu, G. Yu, X. J. Hou, D. Chen and G. Z. Shen, J. Mater. Chem. A, 2013, 1, 2468-2473.
14 (a) J. Zhu and Q. Gao. Microporous Mesoporous Mater., 2009, 124, 144, (b) C. Guan, J. P. Liu, C. W. Cheng, H. X. Li, W. W. Zhou, H. Zhang and H. J. Fan, Energy Environ. Sci., 2011, 4, 4496-4499.
15 G. Zhang and X. W. Lou, Sci. Rep., 2013, 3, 1470.
16 J. Li, S. Xiong, X. Li and Y. Qian, Nanoscale, 2013, 5, 2045.
17 Q. F. Wang, B. Liu, X. F. Wang, S. H. Ran, L. M. Wang, D. Chen and G. Z. Shen, J. Mater. Chem., 2012, 22, 21647-21653.
18 Q. F. Wang, J. Xu, X. F. Wang, B. Liu, X. J. Hou, G. Yu, P. Wang, D. Chen and G. Z. Shen, ChemElectroChem., 2014, 1, 559-564.
19 H. Y. Chen, X. H. Chen, Y. Zeng, S. L. Chen and J. D. Wang, RSC Adv., 2015, 5, 70494-70497.
20 J. B. Cheng, H. L. Yan, Y. Lu, K. W. Qiu, X. Y. Hou, J. Y. Xu, L. Han, X. M. Liu, J. K. Kim and Y. S. Luo, J. Mater. Chem. A, 2015,3, 9769-9776.
21 J. Jia, X. Li and G. Chen, Electrochim. Acta, 2010, 55, 8197-8206.
22 (a) M. D. Koninck and B. Marsan, Electrochim. Acta, 2008, 53, 7012, (b) J. P. Liu, J. Jiang, C. W. Cheng, H. X. Li, J. X. Zhang, H. Gong and H. J. Fan, Adv. Mater., 2011, 23, 2076-2081, (c) A. Pendashteh, S. E. Moosavifard, M. S. Rahmanifar, Y. Wang, M. F. El-Kady, R. B. Kaner and M. F. Mousavi, *Chem. Mater.*, 2015, 27 (11), 3919-3926, (d) L.Huang, J. W. Xiang, W. Zhang, C. J. Chen, H. H. Xu and Y. H. Huang, *J. Mater. Chem. A*, DOI: 10.1039/C5TA05644F, (e) D. Guo, H. M. Zhang, X. Z. Yu, M. Zhang, P. Zhang, Q. H. Li and T. H. Wang, *J. Mater. Chem. A,* 2013, 1, 7247-7254.
23 Y. H. Li, L. J. Cao, L. Qiao, M. Zhou, Y. Yang, P. Xiao and Y. H. Zhang, J. Mater. Chem. A, 2014, 2, 6540-6548.
24 S Abouali, M. A. Garakani, B. Zhang, Z. L. Xu, E. K. Heidari, J. Q. Huang, J. Q. Huang and J. K. Kim, ACS Appl. Mater. Interfaces, 2015, 7, 13503-13511.
25 Z. S.Wu, W. Ren, D. Wang, F. Li, B. Liu and H. M. Cheng, ACS Nano, 2010 , 4 , 5835-5842.
26 S. Chen, J. Zhu, X. Wu, Q Han and X. Wang, ACS Nano, 2010, 4, 2822-2830.
27 X. C. Ren, C. L. Guo, L. Q. Xu, T. T. Li, L. F. Hou and Y. H. Wei, ACS Appl. Mater. Interfaces, 2015, DOI: 10.1021/acsami.5b04094.
28 W. Zilong, Z. Zhu, J. Qiu and S. Yang, J. Mater. Chem. C, 2014 , 2, 1331-1336.
29 X. Lu, M. Yu, G. Wang, T. Zhai, X. Xie, Y. Ling, Y. X. Tong, Y. Li, Adv. Mater., 2012, 25, 267-272.
30 Y. J. Kang, H. Chung, C. H. Han, W. Kim, Nanotechnology, 2012, 23, 065401.
31 M. F. El-Kady, V. Strong, S. Dubin, R. B. Kaner, Science, 2012, 335, 1326-1330.

The porous network $CuCo_2O_4$ nanostructure has been fabricated by a simply spinning method. The asymmetric supercapacitor based on $CuCo_2O_4$ network structure and active carbon delivers a high areal capacitance of 467 mF/cm^2 with a scan rate of 10 mV/s, high energy density of 0.806 mWh/cm^3, also the device demonstrates excellent rate capability and cyclic stability.

Electrospun porous $CuCo_2O_4$ nanowire networks electrode for asymmetric supercapacitor